The Astronomical Journal, 130:586–596, 2005 August

E

NEW CATALOGS OF COMPACT RADIO SOURCES IN THE GALACTIC PLANE

Richard L. White
Space Telescope Science Institute, 3700 San Martin Drive, Baltimore, MD 21218; rlw@stsci.edu

Robert H. Becker
Physics Department, University of California, 1 Shields Avenue, Davis, CA 95616; and Institute of Geophysics and Planetary Physics, Lawrence Livermore National Laboratory, Livermore, CA 94550; bob@igpp.ucllnl.org

and

David J. Helfand
Department of Astronomy, Columbia University, New York, NY 10027; djh@astro.columbia.edu
Received 2005 January 9; accepted 2005 April 17

ABSTRACT

Archival data have been combined with recent observations of the Galactic plane using the Very Large Array to create new catalogs of compact centimetric radio sources. The 20 cm source catalog covers a longitude range of $-20° < l < 120°$; the latitude coverage varies from $\pm0\overset{\circ}{.}8$ to $\pm2\overset{\circ}{.}7$. The total survey area is $\sim$331 deg^2; coverage is 90% complete at a flux density threshold of $\sim$14 mJy, and over 5000 sources are recorded. The 6 cm catalog covers 43 deg^2 in the region $-10° < l < 42°$, $|b| < 0\overset{\circ}{.}4$ to a 90% completeness threshold of 2.9 mJy; over 2700 sources are found. Both surveys have an angular resolution of $\sim$6″. These catalogs provide a 30% (at 20 cm) to 50% (at 6 cm) increase in the number of high-reliability compact sources in the Galactic plane, as well as greatly improved astrometry, uniformity, and reliability; they should prove useful for comparison with new mid- and far-infrared surveys of the Milky Way.

Key words: catalogs — Galaxy: general — H II regions — radio continuum: ISM — supernova remnants — surveys

Online material: machine-readable tables

1. INTRODUCTION

Between 1982 and 1991, the Very Large Array (VLA)[1] was used to conduct extensive snapshot surveys along the plane of the Milky Way at both 6 and 20 cm. In a series of papers in the early 1990s (Becker et al. 1990, 1992, 1994; Zoonematkermani et al. 1990; White et al. 1991; Helfand et al. 1992), we presented catalogs of over 4000 compact ($\theta \leq 25''$) radio sources and used the best far-infrared observations then available (*IRAS*) to construct large samples of compact and ultracompact H II regions, planetary nebulae, etc. Although we employed the best data reduction practices available and tractable on the computers of that era, the images themselves and the source catalogs derived from them left much to be desired. Nonetheless, these data remain the most sensitive radio survey in existence for compact radio emitters in the Galactic plane. The *Midcourse Space Experiment* (*MSX*) mid-infrared survey of the plane (Price et al. 2001; Egan et al. 2003) offers significant improvement in both sensitivity and angular resolution over the largely source-confused *IRAS* images, and the recent launch of the *Spitzer Space Telescope* presages extensive new mid- and far-IR observations of the Milky Way. These developments warrant a new look at the available radio data.

Thus, we have carried out a complete rereduction of the archival VLA data, supplementing the $\sim$3000 individual pointings with 28 hr of new observations designed to correct deficiencies in the existing database. This paper presents new, improved images and catalogs of discrete radio sources at both 6 and 20 cm, as well as unveils a new Web site that makes all the images publicly accessible.

We have also undertaken a new multiconfiguration 20 cm VLA map of the Milky Way (D. J. Helfand et al. 2005, in preparation). The new images are of much higher quality than any previous radio observations of the Galactic plane, but they cover only a portion of the plane ($5° < l < 32°$, $|b| < 0\overset{\circ}{.}6$) at a single wavelength. The older VLA data complement the new survey by extending its area and frequency coverage. While the analysis of the new data is not yet complete, we use it in this paper in several checks of the quality of the images and catalogs presented here.

In § 2 we provide a description of the observations included in this project, while § 3 describes our data analysis, highlighting the differences between the original reductions and our current efforts. The source catalogs, containing over 10,000 entries, comprise § 4, where we also provide descriptions of a number of tests we have performed to quantify the surveys' astrometric and photometric accuracies, as well as highlight the caveats essential for making productive use of these data. Section 5 introduces the Galactic plane Web site,[2] which allows easy access to all images and catalogs and describes some of the uses to which these data products can (and will) be put.

2. OBSERVATIONS

The observations used to construct the catalogs presented herein were taken for a variety of purposes over a period of

[1] The VLA is operated by the National Radio Astronomy Observatory, which is operated by Associated Universities, Inc., under cooperative agreement with the National Science Foundation.

[2] See http://third.ucllnl.org/gps.

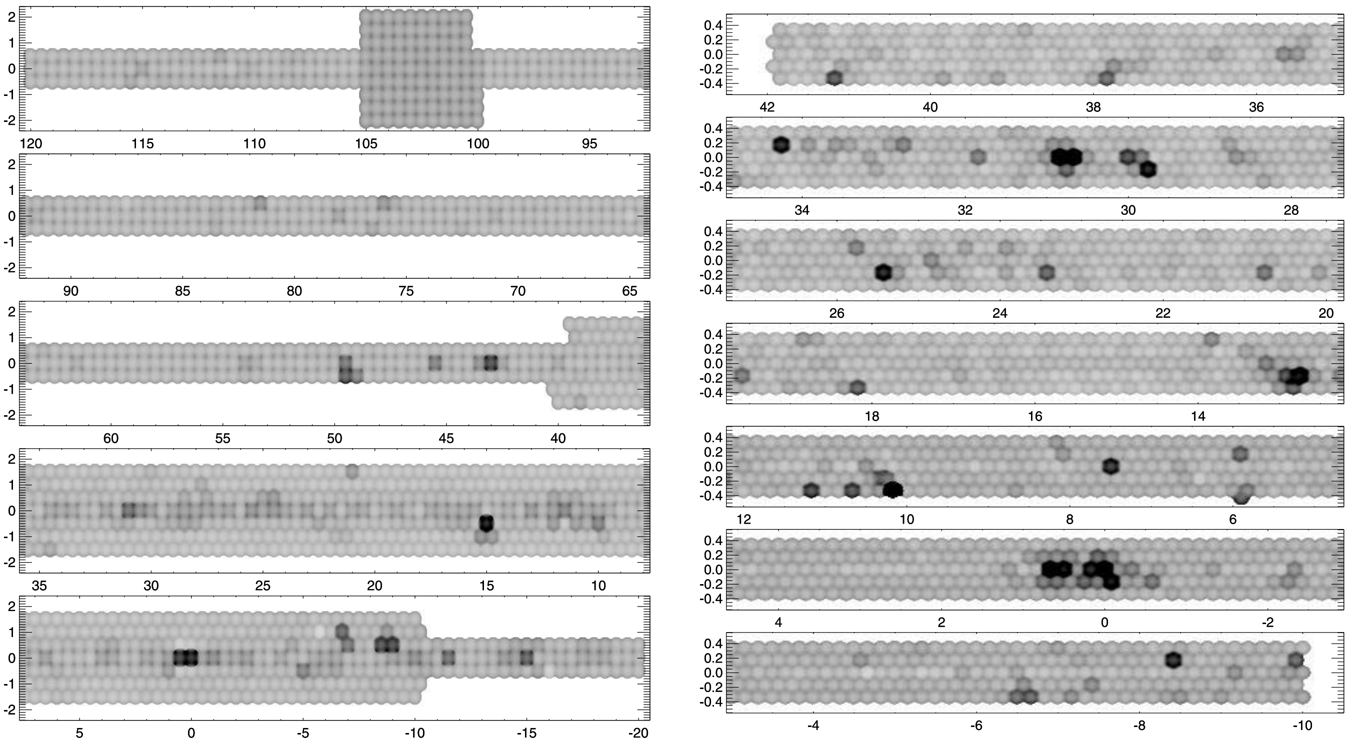

FIG. 1.—Coverage maps at 20 cm (*left*) and 6 cm (*right*). The spatial scales differ for the two panels. Dark regions indicate areas of reduced sensitivity due to elevated noise from bright sources. The pattern of pointing field centers is evident from the lower sensitivity achieved far from the field centers. Note that the oldest 20 cm data (the three inner strips centered on the Galactic plane) did not use staggered pointing positions on alternate rows, which leads to greater variation in the sensitivity.

22 yr in seven of the eight possible VLA configurations. The 20 cm data acquired by other authors between 1982 and 1986 were on a rectilinear grid that provided less-than-optimal coverage (see Fig. 1). Beginning in 1989, we sought, through a series of proposals, to fill out the 20 cm coverage in the Galactic center region and the first two quadrants and to complement these data in the inner Galaxy with a 6 cm snapshot survey. Some of the latter data were corrupted when taken in the original C configuration, and the observations were repeated in 1991, albeit in the lower resolution DnC and D configurations. Furthermore, some of the maps constructed from the salvageable 1990 data were compromised by very bright, extended sources. Given the continuing utility of our compact source catalogs, we reobserved both the low-resolution and compromised fields in the 2004 spring C configuration; these data replace the respective 1990 and 1991 data in the current analysis. We also observed a single field at 20 cm in 2005 February to fill in the only remaining hole in the 20 cm coverage.

All of our analysis reported in this paper focuses on the total intensity maps; we have not attempted to analyze the available polarization data. The 20 cm observations were mainly taken in line mode to avoid the bandwidth-smearing problems that accompany wide-field continuum imaging at that wavelength. Such data do not have associated polarization information, so the available 20 cm polarization data have incomplete sky coverage. The 6 cm observations were taken in continuum mode and could be used to construct polarization images, but they would likely be of limited value, because most of the 6 cm Galactic emission is expected to be thermal and unpolarized. Another obstacle is that the data do not include observations of polarization standard calibration sources. Nonetheless, it might be interesting for a future study to use these same data to examine the polarization properties of Galactic radio sources.

The 20 cm observations taken in 1983 used one intermediate frequency (IF) bandpass at 1611 MHz that included a strong OH maser line. Becker et al. (1992) used these data to construct a catalog of OH masers. For this paper we are interested in radio continuum emission, but it is necessary in the data analysis to account for the OH masers. The self-calibration in particular is complicated by the possibility that a source may have very different flux densities in the two IFs (see § 3.1 below for further discussion).

A summary of the observations used in our final analysis is presented in Table 1. We include the observation dates, configuration, number of fields observed, Galactic longitude range covered, number of bands and bandwidths used, and the central observing frequencies. Most snapshots were of approximately 90 s duration. Over 110 hr of observing time are represented by these observing programs (including fields not used in our final images). The coverage is complete at 20 cm over the range $-20^\circ < l < 120^\circ$; the latitude coverage ranges from $\pm 0\overset{\circ}{.}8$ to $\pm 2\overset{\circ}{.}7$. The 6 cm coverage is complete in the region $-10^\circ < l < 42^\circ$, $|b| \lesssim 0\overset{\circ}{.}4$. Total sky coverage is approximately 331 and 43 deg^2 at 20 and 6 cm, respectively. Figure 1 displays coverage maps in a gray-scale format that illustrates the different extents, pointing grids, and sensitivities of the two surveys.

3. DATA ANALYSIS

Advances in both algorithms and computing power, along with the new observations at 6 cm, allow us to produce significantly improved images and catalogs from these Galactic plane survey data. All the editing, calibration, and subsequent analysis of these data were accomplished using AIPS scripts of our own design employing standard AIPS algorithms. Most of the improvements were taken from the data processing pipeline developed for the FIRST survey (Becker et al. 1995; White et al. 1997). We outline

TABLE 1
Observation Log of 6 and 20 cm Snapshot Data

Date	Configuration	Number of Fields	l Range (deg)	Channels × $\Delta\nu$ (MHz)	Frequency (MHz)
20 cm Observations					
1982 Jul 20	B	96	100–105	1 × 6	1443
1983 Dec 24	BnA	31	340–0	2 × 3	1441/1611
1983 Dec 27	BnA	79	340–0	2 × 3	1441/1611
1983 Dec 30	BnA	241	340–0	2 × 3	1441/1611
1986 Jul 24	B	194	0–100	2 × 3	1441/1641
1986 Jul 25	B	193	0–100	2 × 3	1441/1641
1989 Mar 23	B	29	340–50	2 × 3	1465/1515
1989 Mar 27	B	42	105–120	2 × 3	1465/1515
1989 Apr 29	B	1	357.5	2 × 3	1465
1989 May 1	B	199	350–40	14 × 3	1465
1989 May 2	B	203	350–40	14 × 3	1465
2005 Feb 1	BnA	1	354.25	2 × 25	1451/1490
Total		1309			
6 cm Observations					
1989 Jun 22	C	228	350–18	2 × 50	4840/4890
1990 Sep 26	CnB	139	350–13	...	...
1990 Oct 2	CnB	136	350–13	...	...
1990 Oct 4	CnB	138	350–13	...	...
1990 Oct 15	CnB	145	350–13	...	...
1990 Dec 8	C	255	14–42	...	...
1990 Dec 9	C	257	13–42	...	...
2004 Feb 28	CnB	61	26–40	...	...
2004 Apr 17	C	113	22–42	...	...
2004 Apr 28	C	91	10–42	...	...
Total		1563			

Note.—Only observations used in final map construction are listed; bad data and superseded observations are omitted.

below the significant differences in data processing between the original analysis and the results derived here.

3.1. *Self-Calibration*

No self-calibration was applied in the original analysis. Here we have used several iterations of self-calibration for all fields containing a source "bright enough" to yield significant improvement as defined by the criteria in the AIPS routine *mapit*; more than half of all fields are now self-calibrated. This results in significantly improved dynamic range over a majority of the survey area.

Self-calibration is applied separately to the two frequency channels of 20 cm fields that include OH masers from the catalog of Becker et al. (1992). This is important because the OH maser sources have very different brightnesses in the two bandpasses, leading to errors if the channels are self-calibrated jointly. After self-calibration, the channels are combined and mapped as a single image.

3.2. *Astrometric Distortion Correction*

No corrections were made in the original analysis for the image distortions introduced by approximating the three-dimensional sky as a two-dimensional plane. As noted in Helfand et al. (1992), this produces map source positions offset from true positions by $\sim 3''$ at $20'$ from the pointing center and up to 5 times this value $28'$ off axis; correction factors are calculable from the formula presented in Perley (1989) but were not included in our published catalogs. In the current analysis, the AIPS task *ohgeo* was applied to all images, completely removing these offsets and providing much-improved astrometric accuracy.

3.3. *Image Co-adding*

In the original reduction, we did not take full advantage of the significant overlap in coverage between adjacent images. Here the images have been co-added to maximize sensitivity and minimize variation in the survey sensitivity threshold (see Becker et al. [1995] for a complete discussion of the algorithm employed). Since the observing grid was not optimized for co-adding, however, the rms still rises by a factor of ~ 3 at the boundaries between fields (see Fig. 1 for details).

3.4. *Destriping*

Bright, extended radio sources are severely undersampled by high-resolution, snapshot observations of the type reported here. The common result is large-scale stripes through maps of regions containing or adjacent to bright radio sources. In our original analysis, no attempt was made to account for this nonuniformity in the images. In the current work, we have applied a wavelet algorithm to the images, using a high-pass filter to remove the worst of the striping. The "à trous" wavelet transform (Starck & Murtagh 1994) is used to decompose each field into a stack of images with structures having increasing scale sizes. The sharpest features (point sources) are in the first level of the stack, features larger by a factor of 2 are in the second level, and so on. The decomposition is iterated to remove objects appearing in the sharper channels from the lower resolution levels of the stack, so the last level of the stack contains an estimate of the large-scale "sky" (in this case, stripes from the deconvolution) underlying the sources. Subtracting the smoothest channel from the data removes structures larger than $1\overset{\prime}{.}5$ from the image, which eliminates practically no real features but does a good job in removing the stripes.

3.5. *Source Extraction*

In our original analysis, the source catalogs were constructed by examining each of the ~3000 images by eye and fitting a two-dimensional Gaussian to each source appearing above the local noise level. This labor-intensive technique has the advantage of allowing for an assessment of the reality of each potential source (substantially reducing the number of sidelobes and other map artifacts included as cataloged sources) but suffers from operator error and subjectivity. Having spent considerable effort on the development of an automated source detection algorithm for the FIRST survey (dubbed HAPPY; see White et al. [1997] for details), we have applied this algorithm to our newly reduced images in order to generate the catalogs reported here. Owing to the highly variable noise levels in the plane and our nonuniform coverage, however, we have modified our strategy in running HAPPY: we use a fainter search threshold near field centers where the noise is lower. We accomplish this by running our standard HAPPY algorithm on the same image several times using different-sized windows of included area and different flux density thresholds. This allows us to detect sources down to a 5 σ flux density threshold everywhere in the maps.

3.6. *Sidelobe Probabilities*

The large amount of resolved flux, the high surface density of bright extended sources in the plane, and the modest *u-v* coverage inherent in snapshot observations lead to a significant sidelobe contamination problem. As noted above, our original survey analysis attempted to address this problem by examining each potential source by eye and deciding whether it was a sidelobe. While this approach was reasonably successful, it was far from foolproof;[3] furthermore, the outcome of manual examination is binary—either a source is ignored as a sidelobe or it is included as a catalog source.

In the current analysis we have used an oblique decision tree artificial intelligence algorithm (Murthy et al. 1994) to calculate for each source the probability that it is a sidelobe. We used as a training set for this algorithm a deep, multiconfiguration map of the Galactic plane we are constructing at 20 cm (D. J. Helfand et al. 2005, in preparation; see § 5). To date, this data set covers the region $5^\circ < l < 32^\circ$, $|b| < 0\overset{\circ}{.}8$ (32 deg^2 or ~10% of the existing 20 cm data set) and encompasses 669 of the 20 cm sources detected by HAPPY in the current survey. The angular resolutions of the two surveys are similar. The location of each source in the current catalog was examined by eye in the new, deeper images; missing sources were included as sidelobes in the training set (except for those identified with OH masers in the Becker et al. [1992] catalog; see § 4). Since the threshold of the current catalog is ~10 mJy and that of the new survey images ranges from 1 to 2 mJy (furthermore, the new images have much higher dynamic range and greatly reduced sidelobe levels), there were essentially no ambiguous cases; either a cataloged source was clearly present in the deeper images or the field was blank. While it is conceivable that source variability could explain the presence of a source in the current catalog that was not apparent in the new maps, changes by factors of 5 or more in flux density at 20 cm are extremely rare in both extragalactic and Galactic radio sources; for statistical purposes, it is safe to ignore this possibility.

Of the 669 sources, 122 were identified as sidelobes. The sidelobe fraction is a strong function of source significance: of the sources between 5 and 5.5 σ, nearly two-thirds are likely sidelobes, whereas above 6 σ, this fraction falls to <20% (see Fig. 2). Thus, we present below two catalogs for each data set: a primary catalog with a threshold of 5.5 σ and a "faint source catalog" that extends the catalog to the 5 σ threshold. We selected 5.5 σ as the dividing line since it is at this threshold that most of the sources added to the catalog are real (see Fig. 2). The 5 σ catalog contains many sources (perhaps a majority) that are sidelobes; however, it also includes hundreds of real sources, and in applications such as those that use a match to a catalog at another wavelength as a filter for selecting real sources, the faint source catalog offers a valuable resource (e.g., see Giveon et al. [2005], which presents a match to the mid-IR *MSX* catalog and finds hundreds of new compact and ultracompact H II regions).

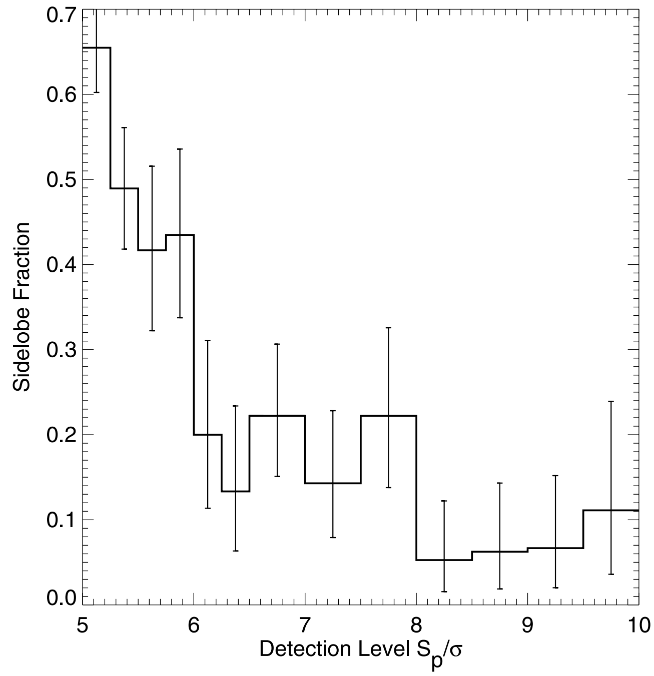

Fig. 2.—Sidelobe fraction vs. detection level S_p/rms for the training set. The fraction is 60% for sources below 5.5 σ and declines to only 0.6% for sources brighter than 10 σ.

Only sources above 5.5 σ are assigned a sidelobe probability. We used the 538 training set sources above 5.5 σ (including 44 sidelobes) to create decision tree classifiers using the OC1 oblique decision tree program (Murthy et al. 1994). The 15 parameters used for the classification include source properties (peak-to-integrated flux ratios, rms noise levels, source major and minor axes compared with the beam, etc.) and properties of the nearest bright source that could be creating sidelobes (positional offsets, flux ratios, etc.). Ten independent decision trees were trained using the randomized search method, and the weighted classifications from those trees were combined to obtain a sidelobe probability estimate using the same approach as that adopted by White et al. (2000). The accuracy of the classification and the probability estimates were confirmed using five-fold cross-validation (also described in White et al.).

The sidelobe probabilities P_s indicate that 79% of the 20 cm sources are highly reliable ($P_s < 0.1$). An additional 9% are fairly reliable ($0.1 < P_s < 0.25$), 6.0% are unreliable ($0.25 < P_s < 0.5$), and 6.3% are probably sidelobes ($P_s > 0.5$). Overall, we estimate that about 10% of the 5.5 σ 20 cm catalog sources are sidelobes.

[3] Or Becker-proof.

TABLE 2

COMPARISON OF OLD AND NEW CATALOGS

Band (λ)	Survey	References	l (deg)	b (deg)	Original: Number of Sources	Original: Threshold (mJy)	Original: Completeness (%)	New: Number of Sources	New: Threshold (mJy)	New: Completeness (%)
20 cm	I	Zoonematkermani et al. 1990	$-20 < l < 120$	$\|b\| < 0.8$	1992	8–25	75	...	...	...
	II	Helfand et al. 1992	$-10 < l < 40$	$0.8 < \|b\| < 1.8$	1457	5–20	95	...	...	...
	Total				3406[a]			6919 (~5000)[b]	13.8	90
6 cm	III	Becker et al. 1994	$-10 < l < 40$	$\|b\| < 0.4$	1272	2.5–10	98	3283	2.9	90
	+IV	This work	$-10 < l < 40$	$\|b\| < 0.4$ (590 fields)	...	...	...	(~2500)[b]	...	...

[a] As noted in Helfand et al. (1992), 43 sources were common between the two catalogs; the reported total takes this into account.
[b] Approximate number of real sources, excluding sidelobes.

At 6 cm, no comparable "truth set" exists, so it is not possible to train our decision tree algorithm to recognize sidelobes. The notion of using the new 20 cm images for comparison was explored, but given the possibility (indeed, the certainty) that inverted spectrum ultracompact H II regions would appear in the 6 cm maps and be absent at 20 cm, we decided to apply the algorithm developed for the 20 cm data with the simple scalings expected for the differences between the 6 and 20 cm images (mainly due to the 5 times lower rms in the 6 cm images, which allows considerably fainter sources to create sidelobes). We do not have high confidence in this approach, and we advise caution when interpreting the 6 cm sidelobe probabilities. Again, we present two catalogs, one with a threshold of 5.5 σ and a faint source compendium reaching to the 5 σ threshold.

3.7. *Summary*

The net result of all these improvements is an increase in the number of detected 5.5 σ sources from 3406 to 5084 at 20 cm (4006 with low sidelobe probabilities, $P_s < 0.1$, of which 28% are newly detected sources) and from 1272 to 2729 at 6 cm (1986 with low sidelobe probabilities, of which 47% are new), along with significant improvements in coverage uniformity, survey sensitivity, and astrometric accuracy. The comparison between the old and new catalogs is summarized in Table 2.

4. THE SURVEY RESULTS

4.1. *Four Catalogs*

In Tables 3–6 we present our new catalogs of compact radio sources in the Galactic plane. Table 3 is a complete list of the 5084 20 cm sources detected at a significance of >5.5 σ. We include the Galactic longitude and latitude, right ascension (J2000.0), declination (J2000.0), peak and integrated flux densities, computed rms in the map at the source position, major and minor axes and position angles derived from elliptical Gaussian fits, the name of the field containing the source, and the probability that the source is a sidelobe. The final column contains a flag "o" indicating whether the source was in our original catalog (Zoonematkermani et al. 1990; Helfand et al. 1992). In addition, 19 sources in Table 3 and one in Table 4 have "OH" flags indicating that they are not continuum sources but instead are detected through their 1611 MHz OH maser emission (Becker et al. 1992). In Table 4 we include the same information (excluding the sidelobe probability) for the 1835 sources falling between 5.0 and 5.5 σ. Again, we emphasize that roughly 60% of these sources are likely to be sidelobes; this faint source catalog should only be used in conjunction with other catalogs that help filter out the true sources.

The 6 cm survey covers only ~13% of the 20 cm survey area but is about 5 times deeper than the 20 cm survey. All 20 cm sources with spectral indices less steep than $\alpha = -1.35$ (where $S_\nu \propto \nu^\alpha$)—the vast majority of all Galactic and extragalactic objects—should have a 6 cm counterpart. Thus, in presenting the catalogs for the 6 cm survey, we include columns recording the 20 cm peak and integrated flux densities, the computed map rms, and the sidelobe probability. Table 5 presents the 2729 sources detected at greater than 5.5 σ significance. It also includes the 179 20 cm sources that fall in the 6 cm survey area but lack 6 cm counterparts (discussed further below). Three of the sources in Table 5 are fainter than 5.5 σ at 6 cm but have 20 cm counterparts, which in our judgment makes them reliable, and we include them here. And five 6 cm sources in the table are listed twice because they match two 20 cm counterparts within 10″. In total the table has 2916 entries.

The columns in Table 5 are similar to those in Tables 3 and 4 with the addition of the 20 cm data. The rms flux density is listed for both surveys even when a source is not present at both wavelengths. The position and field name come from the 6 cm survey except for 20 cm–only sources. The flag indicating whether a source was in the original catalog (last column) here has four possible values: "c" (in the old 6 cm catalog), "l" (in the old 20 cm catalog), "cl" (in both catalogs), and blank (in neither catalog). The "OH" flag is repeated here for masers (none of which are detected at 6 cm). The flag also has an asterisk for a few 20 cm–only sources very close to the 6 cm survey edge (see below).

Table 6 lists the 551 5.0–5.5 σ 6 cm sources whose reliability is less certain. Its columns are identical to those in Table 4. None of these sources have 20 cm counterparts, since the few low-reliability sources with matches are included in Table 5.

4.2. *Quality Assessment*

We have examined by eye the 114 20 cm sources lacking 6 cm counterparts that fall within the region covered by our new, deep, multiarray survey. Of these, 55 (48%) are in regions of diffuse emission where the source detection algorithm has chosen a different component structure at the two frequencies; in such cases, nearby catalog entries should be considered as a single source complex. Of these sources, 12 fall in the $S_p < 5.5$ σ sample, while 41 of the remaining 43 (95%) have, appropriately, low

TABLE 3

20 cm Sources with $S_p > 5.5\ \sigma$

Name ($l + b$)	R.A. (J2000.0)	Decl. (J2000.0)	P_s[a]	S_p (mJy)	S_i (mJy)	σ_S (mJy)	Major Axis (arcsec)	Minor Axis (arcsec)	P.A. (deg)	Field Name	Notes[b]
26.280−0.932	18 42 35.605	−06 20 39.03	0.41	4.59	5.61	0.729	3.79	1.25	21.9	262−10	
26.317+0.410	18 37 51.951	−05 41 48.92	0.02	26.14	30.34	1.408	2.51	0.00	108.8	265+05	o
26.318+0.412	18 37 51.677	−05 41 39.67	0.02	14.02	15.35	1.394	2.62	0.00	74.0	265+05	o
26.318−1.673	18 45 19.304	−06 38 53.45	0.54	8.01	4.61	1.361	1.11	0.00	82.6	265−15	
26.327−1.531	18 44 49.720	−06 34 33.36	0.02	162.39	173.04	0.891	1.87	0.00	51.6	265−15	o
26.345+1.316	18 34 40.922	−05 15 19.14	0.02	19.07	27.68	1.264	4.13	2.04	59.8	265+15	o
26.367−0.905	18 42 39.619	−06 15 16.35	0.02	23.49	30.41	0.895	5.02	0.00	30.6	265−05	o
26.367−0.902	18 42 38.840	−06 15 09.85	0.02	8.40	7.20	0.903	2.50	0.00	73.9	265−05	o
26.377+1.730	18 33 15.934	−05 02 11.38	0.03	10.65	11.76	1.580	3.51	0.00	68.2	265+15	
26.381+1.678	18 33 27.499	−05 03 23.00	0.02	12.88	8.59	1.165	0.00	0.00	78.1	260+15	o
26.382+0.971	18 35 59.048	−05 22 51.66	0.02	6.48	6.67	0.859	2.82	0.00	72.0	267+10	o
26.398−0.498	18 41 15.736	−06 02 25.96	0.02	13.30	13.65	0.977	2.07	0.00	158.7	265−05	o
26.428−0.044	18 39 41.614	−05 48 20.76	0.02	15.55	15.57	1.770	1.28	0.00	34.4	265+00	o, OH
26.430−1.684	18 45 33.791	−06 33 14.26	0.02	17.84	17.39	1.038	2.47	0.00	76.7	260−15	o
26.436+0.059	18 39 20.351	−05 45 06.18	0.02	75.42	102.64	1.786	4.50	2.18	170.8	265+00	o
26.436+0.826	18 36 36.063	−05 23 58.21	0.02	24.40	27.67	1.442	3.06	0.00	70.1	262+10	o
26.448+1.743	18 33 21.142	−04 58 02.78	0.02	11.90	57.90	1.441	14.63	6.59	133.7	265+15	o
26.450−1.285	18 44 10.280	−06 21 14.55	0.02	7.32	7.66	1.136	4.98	0.00	62.7	267−10	
26.451−0.937	18 42 55.763	−06 11 39.68	0.69	6.12	3.61	1.065	0.77	0.00	86.3	267−10	
26.452+0.560	18 37 34.666	−05 30 28.48	0.78	6.68	66.05	0.970	18.89	12.57	106.9	265+05	
26.460−0.050	18 39 46.411	−05 46 48.17	0.14	9.62	15.94	1.708	5.81	2.79	152.4	265+00	
26.479+1.648	18 33 44.899	−04 59 01.77	0.49	4.76	12.73	0.861	7.08	6.02	108.6	270+15	
26.494+1.578	18 34 01.516	−05 00 07.67	0.24	4.21	2.85	0.711	2.79	0.00	84.0	265+15	
26.495−1.749	18 45 54.984	−06 31 29.97	0.36	8.77	6.40	1.415	2.07	0.00	73.4	265−15	
26.509−0.567	18 41 42.623	−05 58 22.27	0.62	5.05	3.97	0.908	3.67	0.00	97.6	265−05	

Notes.—Table 3 is published in its entirety in the electronic edition of the *Astronomical Journal*. A portion is shown here for guidance regarding its form and content. Units of right ascension are hours, minutes, and seconds, and units of declination are degrees, arcminutes, and arcseconds.

[a] P_s is the probability that the source is a sidelobe of a nearby bright object (see the text for details).

[b] Source notes: "o" indicates that the source was in the original catalogs of Zoonematkermani et al. (1990) or Helfand et al. (1992). "OH" indicates sources detected through 1611 MHz OH maser emission rather than 20 cm continuum emission (Becker et al. 1992).

TABLE 4

20 cm Sources with $S_p < 5.5\ \sigma$

Name ($l + b$)	R.A. (J2000.0)	Decl. (J2000.0)	S_p (mJy)	S_i (mJy)	σ_S (mJy)	Major Axis (arcsec)	Minor Axis (arcsec)	P.A. (deg)	Field Name	Notes[a]
24.819−1.161	18 40 43.438	−07 44 52.85	5.09	5.99	1.018	4.80	0.00	66.4	247−10	
24.835−1.002	18 40 11.041	−07 39 38.81	3.95	4.39	0.761	3.61	0.00	52.2	247−10	
24.839−1.442	18 41 46.166	−07 51 28.58	4.81	8.14	0.953	5.96	0.00	78.6	250−15	
24.846−1.485	18 41 56.353	−07 52 17.68	4.83	4.10	0.896	2.85	0.00	78.5	250−15	
24.847−1.638	18 42 29.230	−07 56 27.17	6.23	6.55	1.169	6.23	0.00	88.6	250−15	
24.849+0.087	18 36 18.318	−07 08 54.78	12.44	154.02	2.331	23.36	13.50	153.6	250+05	
24.874−1.642	18 42 33.105	−07 55 08.55	5.89	6.31	1.077	5.48	0.00	92.3	250−15	
24.881+1.056	18 32 53.935	−06 40 26.35	4.94	3.89	0.907	2.06	0.00	81.2	250+15	
24.887−1.178	18 40 54.631	−07 41 43.83	6.31	5.77	1.238	4.36	0.00	76.5	252−10	
24.902+1.230	18 32 19.037	−06 34 31.23	6.77	4.39	1.353	1.68	0.00	78.4	247+10	
24.907+1.057	18 32 56.697	−06 39 00.51	5.18	5.98	0.967	4.13	0.00	92.3	250+15	
24.938+0.883	18 33 37.508	−06 42 11.41	6.36	4.74	1.217	2.72	0.00	86.0	247+10	
24.968+1.642	18 30 58.162	−06 19 35.47	4.20	5.91	0.818	6.93	0.00	87.7	250+15	
25.026+1.562	18 31 21.837	−06 18 43.05	3.62	3.56	0.670	5.61	0.00	81.7	250+15	
25.046+0.673	18 34 34.486	−06 42 15.75	12.41	33.33	2.409	8.22	4.43	77.5	252+10	o
25.111−1.027.....................	18 40 47.004	−07 25 35.95	4.85	6.71	0.942	5.09	0.00	67.1	252−10	
25.168−0.923	18 40 31.009	−07 19 43.40	4.42	13.63	0.878	15.14	0.00	128.5	247−10	
25.169+1.595	18 31 30.709	−06 10 11.24	5.02	5.81	0.963	5.27	0.00	73.4	255+15	
25.172−1.213	18 41 33.625	−07 27 28.03	7.08	5.94	1.328	2.64	0.00	56.3	252−10	
25.201−0.945	18 40 39.303	−07 18 34.62	4.41	5.96	0.808	6.73	0.00	98.9	252−10	
25.289+1.610	18 31 40.786	−06 03 23.71	5.71	3.90	1.138	1.63	0.00	76.7	255+15	
25.351−1.409.....................	18 42 35.714	−07 23 17.40	4.56	4.18	0.908	3.73	0.00	65.9	255−15	
25.429+0.887	18 34 31.281	−06 15 55.24	6.23	4.48	1.199	3.59	0.00	76.8	252+10	
25.444−0.853	18 40 46.378	−07 03 06.05	7.41	14.57	1.423	10.71	0.00	75.8	255−05	
25.463−1.248	18 42 13.407	−07 12 52.65	6.88	25.44	1.366	17.57	1.36	139.2	252−10	

Notes.—Table 4 is published in its entirety in the electronic edition of the *Astronomical Journal*. A portion is shown here for guidance regarding its form and content. Units of right ascension are hours, minutes, and seconds, and units of declination are degrees, arcminutes, and arcseconds.

[a] Source notes: "o" indicates that the source was in the original catalogs of Zoonematkermani et al. (1990) or Helfand et al. (1992). "OH" indicates sources detected through 1611 MHz OH maser emission rather than 20 cm continuum emission (Becker et al. 1992).

TABLE 5

6 cm SOURCES WITH $S_p > 5.5\ \sigma$

NAME ($l + b$)	R.A. (J2000.0)	DECL. (J2000.0)	6 cm DATA P_s[a]	S_p (mJy)	S_i (mJy)	σ_S (mJy)	Major Axis (arcsec)	Minor Axis (arcsec)	P.A. (deg)	20 cm DATA P_s[a]	S_p (mJy)	S_i (mJy)	σ_S (mJy)	FIELD NAME	NOTES[b]
354.829+0.077	17 32 25.653	−33 16 08.52	0.02	10.32	16.24	0.365	6.18	3.24	170.4	...	...	...	1.464	35483+00	c
354.832−0.409	17 34 23.112	−33 31 53.60	...	...	...	0.457	...	...	...	0.62	23.42	29.85	4.091	3550+00	
354.871−0.006	17 32 52.111	−33 16 48.21	0.02	4.25	5.72	0.217	4.37	0.00	119.1	...	...	...	1.136	35483+00	c
354.871−0.012	17 32 53.513	−33 16 56.58	0.02	1.78	3.69	0.221	8.62	4.01	156.8	...	...	...	1.130	35483+00	c
354.892+0.025	17 32 47.954	−33 14 40.43	0.02	5.44	11.91	0.287	7.05	5.51	159.1	...	...	...	1.069	35483+00	c
354.934+0.329	17 31 41.623	−33 02 36.55	...	...	...	0.371	...	...	...	0.02	9.67	44.23	1.329	3550+05	
354.936+0.328	17 31 41.990	−33 02 32.90	0.02	9.34	82.72	0.358	21.13	11.79	86.4	...	...	...	1.347	35500+33	
354.937+0.330	17 31 41.881	−33 02 27.48	0.02	9.19	145.08	0.354	26.03	20.06	145.8	...	...	...	1.340	35483+33	
354.938+0.333	17 31 41.294	−33 02 16.15	0.02	17.45	50.52	0.347	10.75	5.38	36.8	0.02	34.21	113.57	1.307	35500+33	l
354.939+0.332	17 31 41.734	−33 02 15.71	0.02	40.99	101.75	0.344	8.45	3.26	94.0	...	...	...	1.325	35483+33	c
354.940+0.328	17 31 42.732	−33 02 19.73	0.02	16.26	72.15	0.341	18.40	6.50	166.5	0.02	16.36	85.77	1.316	35483+33	
354.963+0.016	17 33 01.371	−33 11 26.00	0.02	5.96	7.14	0.189	5.37	0.00	163.4	...	...	...	0.948	35500+00	c
354.973+0.416	17 31 26.867	−32 57 47.34	...	...	...	0.614	...	...	...	0.52	6.17	9.31	1.015	3550+05	
354.977+0.304	17 31 54.496	−33 01 16.61	0.02	10.24	10.33	0.272	1.88	0.00	170.7	0.02	22.07	32.38	1.360	35500+33	cl
354.982−0.209	17 33 58.287	−33 17 47.79	0.02	4.84	5.49	0.427	4.00	0.00	40.9	...	...	...	2.412	35500−33	c
355.000−0.027	17 33 17.461	−33 10 59.04	0.02	4.50	5.62	0.169	5.95	0.60	167.1	...	...	...	0.940	35500+00	c
355.008−0.195	17 33 59.039	−33 16 01.76	0.14	2.39	1.80	0.396	2.11	0.00	76.5	...	...	...	2.107	35500−33	
355.068−0.303	17 34 34.527	−33 16 32.86	...	...	...	0.417	...	...	...	0.18	24.92	27.75	3.985	3550+00	
355.105+0.097	17 33 04.043	−33 01 37.75	0.02	9.92	9.15	0.371	0.51	0.00	91.7	0.02	31.30	29.87	1.195	35516+00	cl
355.110−0.028...............	17 33 34.777	−33 05 28.25	0.02	2.54	4.86	0.248	6.16	4.78	21.0	...	...	...	1.080	35516+00	
355.112−0.023...............	17 33 33.832	−33 05 11.48	0.52	1.43	4.82	0.234	13.37	6.38	175.6	...	...	...	1.083	35533+00	
355.127−0.030	17 33 37.849	−33 04 38.63	0.61	1.38	1.54	0.211	2.10	0.00	98.9	...	...	...	1.140	35516+00	
355.129−0.303	17 34 43.966	−33 13 26.00	0.02	10.68	12.45	0.300	2.61	0.85	120.8	...	...	...	4.819	35516−33	c
355.198+0.130	17 33 10.484	−32 55 51.35	0.02	4.68	19.32	0.395	15.63	6.39	31.6	...	...	...	1.797	35533+00	
355.203−0.016	17 33 46.371	−33 00 25.25	0.02	2.32	5.39	0.190	7.40	4.21	92.4	...	...	...	1.439	35516+00	c

NOTES.—Table 5 is published in its entirety in the electronic edition of the *Astronomical Journal*. A portion is shown here for guidance regarding its form and content. Units of right ascension are hours, minutes, and seconds, and units of declination are degrees, arcminutes, and arcseconds.

[a] P_s is the probability that the source is a sidelobe of a nearby bright object (see the text for details).

[b] Source notes: "c" indicates that the source was in the original 6 cm catalog of Becker et al. (1994); "l" indicates that the source was in the original 20 cm catalogs of Zoonematkermani et al. (1990) or Helfand et al. (1992); "OH" indicates sources detected through 1611 MHz OH maser emission rather than 20 cm continuum emission (Becker et al. 1992).

TABLE 6
6 cm SOURCES WITH $S_p < 5.5\ \sigma$

Name ($l + b$)	R.A. (J2000.0)	Decl. (J2000.0)	S_p (mJy)	S_i (mJy)	σ_S (mJy)	Major Axis (arcsec)	Minor Axis (arcsec)	P.A. (deg)	Field Name	Notes[a]
22.727+0.269	18 31 42.065	−08 56 52.20	1.77	1.69	0.341	4.40	0.00	83.2	2283+33	
22.749+0.308	18 31 36.236	−08 54 37.57	1.51	1.79	0.291	5.84	0.00	75.3	2266+33	
22.750−0.248	18 33 36.141	−09 09 57.64	1.37	4.11	0.273	11.88	5.85	165.3	2283+00	
22.761−0.239	18 33 35.448	−09 09 09.21	1.22	1.54	0.232	4.81	0.00	105.1	2266−33	
23.186+0.162	18 32 56.515	−08 35 25.47	1.14	2.22	0.224	9.39	0.00	70.9	2316+33	
23.203+0.142	18 33 02.985	−08 35 03.70	1.06	4.98	0.203	13.31	8.24	87.2	2333+33	
23.224−0.137	18 34 05.382	−08 41 40.76	1.05	1.55	0.198	9.27	0.00	167.5	2316−33	
23.435−0.204	18 34 43.347	−08 32 18.40	5.84	18.11	1.092	13.43	5.34	16.9	2350−33	o
23.479+0.069	18 33 49.475	−08 22 22.34	2.48	6.18	0.471	7.13	6.57	39.1	2350+00	
23.621+0.374	18 32 59.781	−08 06 22.03	0.82	0.84	0.164	2.69	0.00	74.1	2366+33	
23.649−0.039	18 34 31.787	−08 16 18.52	0.98	3.61	0.191	20.62	3.62	18.4	2366+00	
23.690+0.342	18 33 14.371	−08 03 35.64	0.63	0.61	0.115	3.68	0.00	79.6	2366+33	
23.747+0.103	18 34 12.141	−08 07 09.18	1.87	2.27	0.353	7.91	0.00	168.0	2383+00	
23.822+0.392	18 33 18.401	−07 55 10.53	1.23	8.98	0.225	16.49	12.77	114.1	2383+33	
24.017+0.238	18 34 13.101	−07 49 05.03	2.05	8.01	0.391	14.69	6.43	150.9	2400+00	
24.112+0.236	18 34 24.256	−07 44 04.33	1.58	6.01	0.290	13.53	3.90	80.7	2400+00	
24.199+0.243	18 34 32.417	−07 39 14.22	1.74	8.63	0.331	17.31	7.85	157.4	2416+00	
24.229+0.120	18 35 02.281	−07 41 02.53	0.93	2.65	0.173	14.59	3.88	19.9	2433+00	
24.363+0.044	18 35 33.554	−07 35 58.98	1.33	9.47	0.247	18.72	11.52	159.4	2433+00	
24.446−0.168	18 36 28.354	−07 37 27.76	0.94	2.43	0.185	8.95	5.47	142.2	2450−33	
24.456−0.352	18 37 09.040	−07 41 59.11	1.41	2.74	0.268	7.77	0.00	84.2	2450−33	
24.748−0.206	18 37 10.158	−07 22 23.62	2.22	2.56	0.413	4.92	0.00	137.0	2483−33	o
24.774+0.187	18 35 48.563	−07 10 10.18	1.12	1.18	0.216	2.38	0.00	104.0	2483+00	
24.814+0.122	18 36 06.960	−07 09 50.03	2.18	3.04	0.435	4.42	0.00	80.0	2483+33	
25.157+0.057	18 36 59.041	−06 53 19.82	1.94	11.65	0.363	29.36	5.30	18.2	2533+00	

NOTES.—Table 6 is published in its entirety in the electronic edition of the *Astronomical Journal*. A portion is shown here for guidance regarding its form and content. Units of right ascension are hours, minutes, and seconds, and units of declination are degrees, arcminutes, and arcseconds.
[a] Source notes: "o" indicates that the source was in the original catalog of Becker et al. (1994).

sidelobe probabilities (<0.25). Seven of the sources are detected in the 20 cm catalog because they are OH masers, which are not expected to have 6 cm continuum emission. A total of 44 (39%) of the 20 cm sources lacking 6 cm counterparts are almost certainly spurious (sidelobes, noise bumps barely above threshold, etc.); of these, 41 (93%) have sidelobe probabilities above 0.25 or are found in the low-reliability ($S_p < 5.5\ \sigma$) sample. Thus, it appears from this comparison data set that using 0.25 as the sidelobe probability threshold is both >90% accurate and >90% complete. The remaining eight 20 cm sources without 6 cm matches do appear in our deep, multiarray 20 cm images. In a few cases, they fall very close to the boundary of the 6 cm coverage where the sensitivity is too low for them to be detected, but the majority of cases are truly steep-spectrum and/or highly variable sources. The former objects are noted with an asterisk in Table 5.

A detailed source-by-source comparison between the old and new 6 cm catalogs was carried out for the region $5^\circ < l < 15^\circ$ using both the 20 and 6 cm images, the new multiarray 20 cm survey images, and the *MSX* images. In this $\sim$8 deg^2 region, 198 6 cm sources appear in the old catalog; 171 (86%) of these are also found in the new catalog, albeit with slightly shifted (and improved) positions and revised flux densities. Of the 27 missing sources, 15 are spurious objects that have disappeared in the reprocessed images, and three are real sources that now simply fall outside the trimmed survey area. Examination of the new 20 cm data shows that five missing sources are actually peaks in a large diffuse region of thermal emission evident in the 20 μm *MSX* map; these are no longer considered significant in the reprocessed high-resolution (and rather noisy) 6 cm image and so do not appear in the new catalog. The final four missing sources are almost certainly real and are present in the images but fall below the formal threshold for acceptance to the catalog.

This same region contains 23 sources from the old 20 cm catalog that had no match in the old 6 cm catalog. Eight are still found in the new 20 cm catalog, with five of those now having counterparts in the new 6 cm catalog. The three without new 6 cm counterparts include an OH maser, a source that falls in the low-sensitivity region at the edge of the 6 cm survey area, and a truly steep-spectrum (or variable) source, 9.001+0.078, that falls just below the threshold for catalog inclusion but is clearly present in the reprocessed 6 cm image. Of the 15 old 20 cm sources that are absent from the new 20 cm catalog, 11 are clearly spurious, since they completely fail to appear in our deep multiarray images. The other four lie in diffuse source complexes that are largely resolved out at 6 cm, although one of those actually does appear in the new 6 cm catalog.

The new 6 cm catalog contains 489 entries with greater than 5.5 σ significance in the $5^\circ < l < 15^\circ$ region, more than double the number of sources in the old catalog. While a number of these new entries represent components of large source complexes previously grouped as one source, there are also many new sources added as a consequence of the new data and improved processing techniques. In summary, then, our revised analysis has removed 26 spurious sources from the old catalog while losing only seven real discrete objects (which can be recovered from examination of the images) and has more than doubled the number of sources and source components detected.

4.3. *Survey Sensitivity*

Because of the variety of observing modes used and the sparse observing grid, the sensitivity over the survey area varies

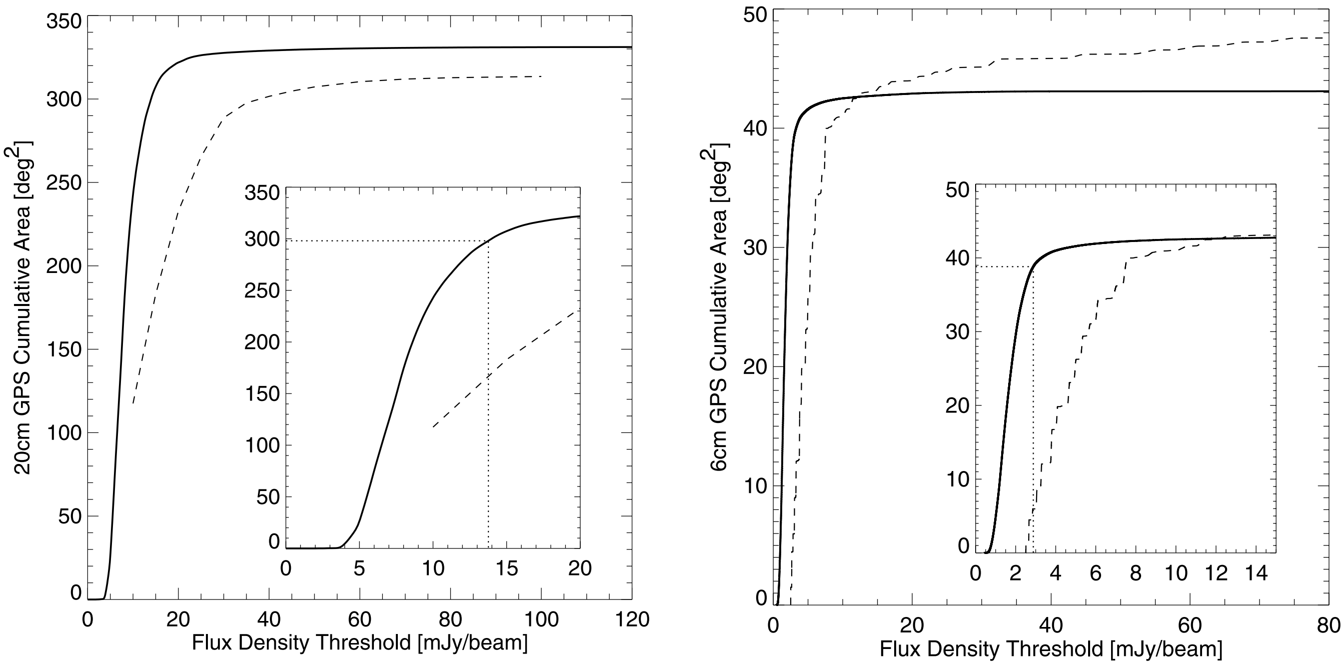

FIG. 3.—Cumulative area functions for the 20 cm (*left*) and 6 cm (*right*) surveys. The *y*-axis is the sky area covered to the given sensitivity limit or better at a 5.5 σ detection threshold. The dashed lines show the coverage from the old versions of these surveys, while the dotted lines indicate the 90% completeness levels.

significantly. The median rms values are 0.897 and 0.179 mJy for the 20 and 6 cm surveys, respectively; with our improved reduction techniques and addition of new data, only $\sim$5% of the fields at both wavelengths exceed these median values by more than a factor of 2 (42 out of 1309 fields at 20 cm and 90 out of 1563 fields at 6 cm). In Figure 3 we show the cumulative coverage for the two surveys as a function of flux density threshold for the high-reliability catalogs. A useful figure of merit to describe the surveys is that 90% of the survey areas have thresholds deeper than 2.9 and 13.8 mJy for 6 and 20 cm, respectively.

Also shown in Figure 3 is the marked improvement in sensitivity that has resulted from our new analysis. The dashed curves represent the cumulative coverage of the original surveys. Two points are worth noting. First, for the 6 cm survey, it is clear that the total effective area in the old analysis exceeds that in the new at high flux density thresholds (>10–20 mJy). This is a consequence of the fact that we have trimmed the edges of the survey region, dropping all areas in which the sensitivity falls to less than $\sim$10% of the on-axis value; a total of 56 sources appearing in the old catalog—all with poorly determined positions and flux densities because they are far from a pointing center—are dropped in the new catalog. A few of these sources actually appear in our new images but are not in the catalog as a consequence of the fact that the HAPPY source detection algorithm excludes sources if their source extraction island intersects the boundary of the image. More importantly, the lower flux density thresholds of the current analysis are apparent in the figure. In Figure 4 we quantify the change for the 6 cm survey by plotting the cumulative sky area as a function of the flux detection threshold ratio of the new maps compared to the old. Fully 40% of the survey area shows a factor of 3 improvement, while 90% gains at least a factor of 2.

4.4. *Survey Astrometry*

As noted in § 3.2, a major improvement in the new catalogs is the inclusion of a correction for the distortion introduced into VLA images by mapping the three-dimensional sky onto a two-dimensional image; some sources in the original catalogs had astrometric errors exceeding 5″ as a consequence of this effect. A simple assessment of the astrometric accuracy of the current catalogs is provided by examining the offsets between the point sources (major axes <5″) found in both catalogs. We display this comparison in Figure 5. The rms position discrepancies are 0.″64 in right ascension and 0.″81 in declination. Since uncertainties in both positions are included in this comparison, we infer that the rms position errors for the individual catalogs are $\Delta\alpha = 0.''45$ and $\Delta\delta = 0.''57$. Even these values should be treated as upper limits, since spectral index variability over even compact sources can induce centroid shifts that masquerade as astrometric errors.

A further test of the astrometry comes from comparing our positions to the deep multiconfiguration data set described above. There are 212 sources at 20 cm and 300 sources at 6 cm that match nearly pointlike sources in the new catalog. The rms

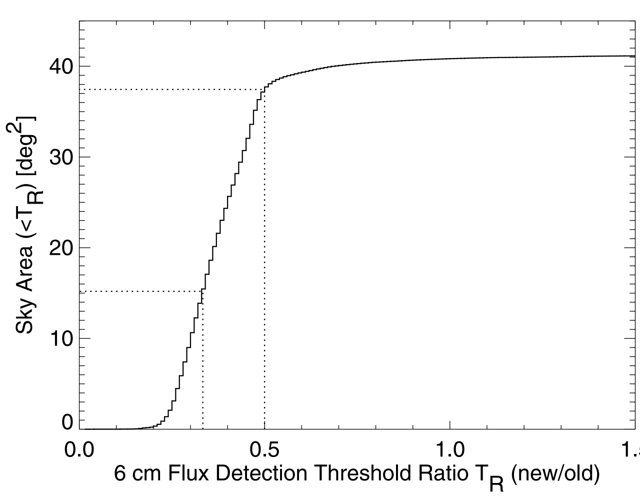

FIG. 4.—Improvement in the flux density detection limits for the 6 cm survey. The dotted lines indicate factors of 2 and 3 improvement in sensitivity.

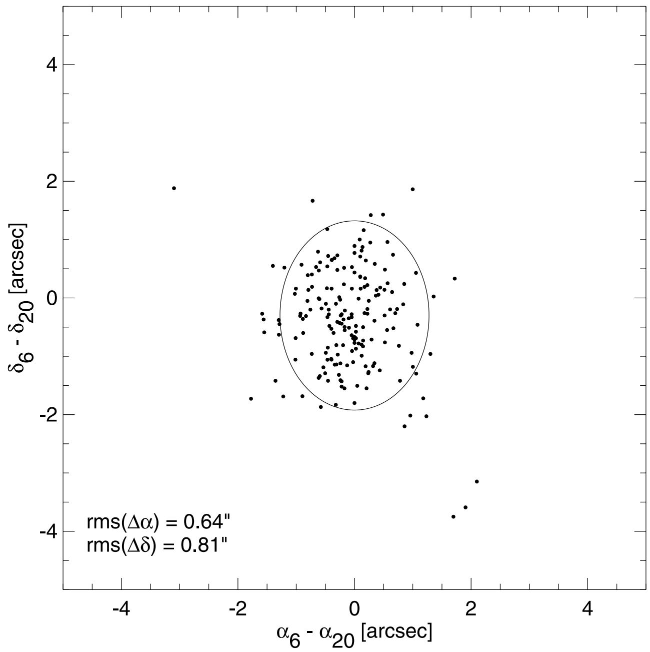

FIG. 5.—Position differences for sources appearing in both the 6 and 20 cm surveys. Only sources that are compact with deconvolved major axes smaller than 5″ are included. The 2 σ error ellipse is shown. The scatter is larger in declination because of the extension of the synthesized VLA beam in the north-south direction at southern declinations.

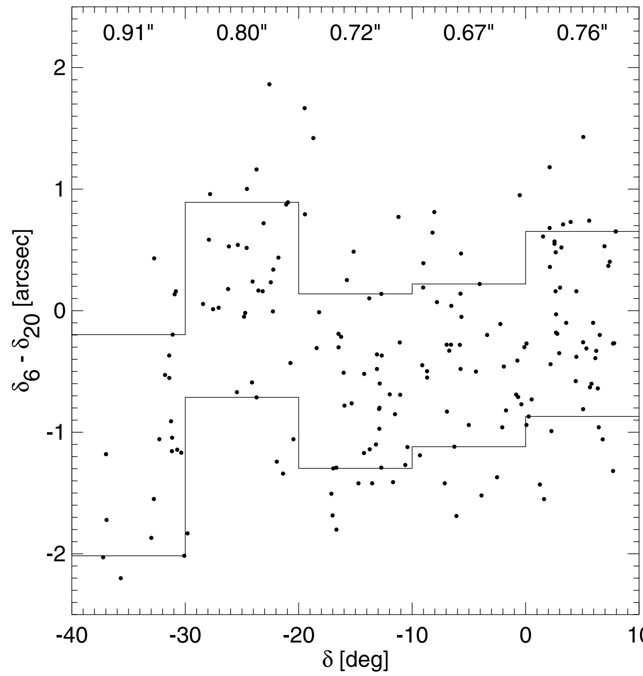

FIG. 6.—Difference between 6 and 20 cm declinations as a function of source declination. The lines indicate the ± 1 σ range about the mean, and the numbers at the top give the value of σ for each bin. The increase in the uncertainty for more southerly sources is apparent, as is a small systematic offset of $\sim 0\farcs25$ between the two catalogs.

positional errors for the 20 cm catalog are $\Delta\alpha = 0\farcs67$, $\Delta\delta = 0\farcs78$ and for the 6 cm catalog are $\Delta\alpha = 0\farcs67$, $\Delta\delta = 0\farcs84$. These are consistent with the values quoted above given that the deeper survey also has positional errors. The median position offsets between the two surveys are $\Delta\alpha = -0\farcs05$, $\Delta\delta = 0\farcs10$ (20 cm) and $\Delta\alpha = -0\farcs04$, $\Delta\delta = -0\farcs14$ (6 cm).

The greater positional uncertainty in declination is occasioned by the fact that the VLA synthesized beam is elongated in the north-south direction when observing sources at southerly declinations; this effect is apparent in Figure 6, where it is seen that the scatter in declination increases by $\sim$30% going from sources with $\delta > -10°$ to the southern limit of the survey at $\delta \sim -37°$. Also apparent in this figure is a $\sim 0\farcs25$ shift to the south for the 20 cm catalog with respect to the 6 cm catalog; the comparison to our new deep survey shows that the offsets for the two surveys are both approximately $0\farcs1$ but in opposite directions. This sets the absolute astrometric accuracy of the catalogs presented here. The origin of these small shifts is unclear, and further tests are under way to understand it.

4.5. *Survey Photometry*

We expect the photometry in these catalogs to be superior to the original analysis because the noise in the maps is reduced. We have checked the photometric accuracy of the 20 cm catalog using point-source counterparts in the deep multiconfiguration catalog (see above). The results are shown in Figure 7. The general agreement between flux densities in the two surveys is good. The scatter is clearly asymmetric, with flux densities from this paper's catalog tending to fall below those from the multiconfiguration catalog. This can be attributed to the tendency of our single-configuration snapshot observations to resolve out flux from slightly extended sources. The "CLEAN bias" effect also reduces the flux densities of fainter sources in snapshot surveys (White et al. 1997). We have not attempted to correct for the CLEAN bias (as we did for the FIRST survey), since we lack the data to model the effect accurately in these complex, highly variable maps. But users of the catalog should be cognizant of the likely underestimate of flux densities in the catalog due to the bias.

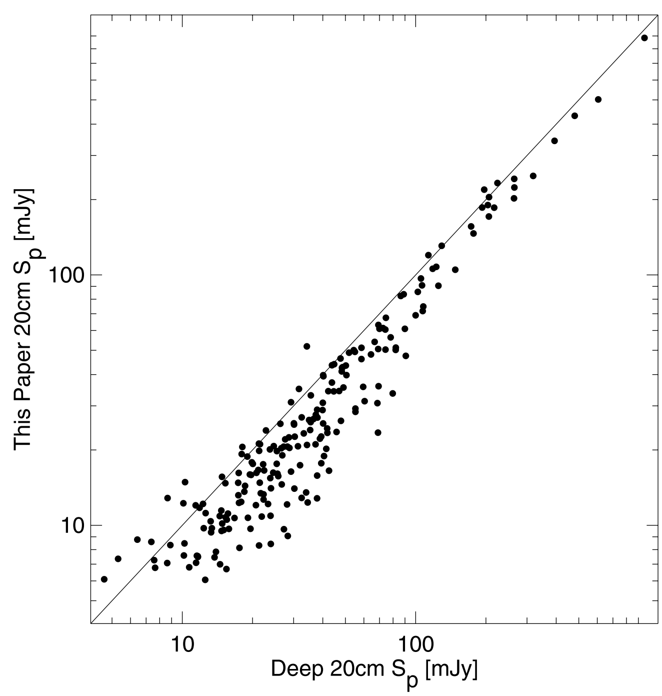

FIG. 7.—Comparison of 20 cm flux densities from this paper to a deep multiconfiguration catalog for 212 compact sources. The agreement is good. The distribution is skewed toward fainter flux densities in this paper's catalog because the multiconfiguration images recover more flux from slightly extended sources and do not suffer from CLEAN bias.

5. THE GALACTIC PLANE WEB SITE

While catalogs are a convenient and compact form in which to present the primary results of these surveys, the images themselves are also of great utility. In addition to their use in making overlays with observations at different wavelengths and in assessing the validity of a given catalog entry, the vast majority of the more than two billion pixels comprising the images are noise—but not noise without content. Each of the 235 million beam areas that does not contain a source provides an upper limit to the radio flux density for any object at that location. Furthermore, stacking this "noise" at the locations of many sources identified in another wavelength band can provide the mean radio flux density for the source class in question to levels far below the typical image rms (e.g., Glikman et al. 2004).

Consistent with our past practice of providing user-friendly access to source images and catalogs (e.g., our VLA FIRST survey), we are making all these images available on the MAGPIS Web site.[4] The Multi-Array Galactic Plane Imaging Survey collects, as its namesake is wont to do, bits and pieces of the Galactic sky that have been imaged at high resolution. At its inception, the site included the 6 and 20 cm data described here, as well as the main MAGPIS database, which currently includes high dynamic range, high-sensitivity images for the region $5^\circ < l < 32^\circ$, $|b| < 0\overset{\circ}{.}6$ (D. J. Helfand et al. 2005, in preparation). Much of this latter area is being imaged with *XMM-Newton* at hard X-ray wavelengths, and all of it has been mapped at mid-infrared wavelengths by *MSX*; mosaics of the latter data, gridded onto the same coordinate system as the radio images, are included at this site, as will be the X-ray data as they become available. The high-resolution, high-sensitivity GLIMPSE Legacy Project, currently being conducted with the *Spitzer Space Telescope*, includes much of the same region of sky and will undoubtedly increase significantly the value of these radio images.

Even though this work comprises a Galactic survey, there is a substantial admixture of extragalactic sources. At a threshold peak flux density of $S_{20\ \rm cm} = 13.8$ mJy, our 90% completeness threshold, the FIRST survey (Becker et al. 1995)—a high-latitude extragalactic survey with similar angular resolution—predicts 9.0 extragalactic radio sources deg^{-2}, compared with the 10.3 sources deg^{-2} with $S_p > 13.8$ mJy in the 20 cm catalog presented here. Even in the Galactic plane, then, 88% of the compact radio sources are extragalactic. In some cases extragalactic sources can be classified as such by their morphology (e.g., radio doubles), but for the most part selecting out the Galactic sources requires multiwavelength follow-up observations. The combination of these VLA data with the near-IR (Two Micron All Sky Survey), mid- and far-IR (*MSX* and *Spitzer*), and X-ray (*XMM-Newton*) databases now being assembled promises a substantially improved view of the source populations and activity in Galactic regions obscured from view at visible wavelengths.

R. H. B. and D. J. H. acknowledge the support of the National Science Foundation under grants AST 02-6309 and AST 02-655, respectively. R. H. B.'s work was supported in part under the auspices of the US Department of Energy by Lawrence Livermore National Laboratory under contract W-7405-ENG-48. D. J. H. was also supported in this work by NASA grant NAG5-13062. R. L. W. acknowledges the support of the Space Telescope Science Institute, which is operated by the Association of Universities for Research in Astronomy, Inc., under NASA contract NAS5-26555.

[4] See http://third.ucllnl.org/gps.

REFERENCES

Becker, R. H., White, R. L., & Helfand, D. J. 1995, ApJ, 450, 559
Becker, R. H., White, R. L., Helfand, D. J., & Zoonematkermani, S. 1994, ApJS, 91, 347
Becker, R. H., White, R. L., McLean, B. J., Helfand, D. J., & Zoonematkermani, S. 1990, ApJ, 358, 485
Becker, R. H., White, R. L., & Proctor, D. D. 1992, AJ, 103, 544
Egan, M. P., Price, S. D., & Kraemer, K. E. 2003, BAAS, 203, 5708
Giveon, U., Becker, R. H., Helfand, D. J., & White, R. L. 2005, AJ, 129, 348
Glikman, E., Helfand, D. J., Becker, R. H., & White, R. L. 2004, in ASP Conf. Ser. 311, AGN Physics with the Sloan Digital Sky Survey, ed. G. T. Richards & P. B. Hall (San Francisco: ASP), 351
Helfand, D. J., Zoonematkermani, S., Becker, R. H., & White, R. L. 1992, ApJS, 80, 211
Murthy, S. K., Kasif, S., & Salzberg, S. 1994, J. Artif. Intell. Res., 2, 1
Perley, R. A. 1989, in ASP Conf. Ser. 6, Synthesis Imaging in Radio Astronomy, ed. R. A. Perley, F. R. Schwab, & A. H. Bridle (San Francisco: ASP), 259
Price, S. D., Egan, M. P., Carey, S. J., Mizuno, D. R., & Kuchar, T. A. 2001, AJ, 121, 2819
Starck, J., & Murtagh, F. 1994, A&A, 288, 342
White, R. L., Becker, R. H., & Helfand, D. J. 1991, ApJ, 371, 148
White, R. L., Becker, R. H., Helfand, D. J., & Gregg, M. D. 1997, ApJ, 475, 479
White, R. L., et al. 2000, ApJS, 126, 133
Zoonematkermani, S., Helfand, D. J., Becker, R. H., White, R. L., & Perley, R. A. 1990, ApJS, 74, 181